Title
Implementation of an LED-based clinical spatial frequency domain imaging system

ISBN
9780819488978

Authors
Mazhar, Amaan
Sharif, Seyed A
Saggese, Steve
et al.

Publication Date
2012-02-09

DOI
10.1117/12.909813

Implementation of an LED based Clinical Spatial Frequency Domain Imaging System

Amaan Mazhar[1], Seyed A. Sharif[1], Steve Saggese[2], Bernard Choi[1], David J. Cuccia[2], Anthony J. Durkin[1]

[1] Beckman Laser Institute. University of California - Irvine.

[2] Modulated Imaging Inc. Irvine, CA

Abstract

Spatial Frequency Domain Imaging (SFDI) is a non-contact imaging method that uses multiple frequency spatial illumination to generate two dimensional maps of tissue optical properties (absorption and reduced scattering) and chromophore concentrations. We present phantom validation and pilot clinical data of a deployed light-emitting diode (LED) based system. The system employs four LED wavelengths (658 nm, 730 nm, 850 nm, 970 nm) to quantitatively assess tissue health by measurement of common tissue constituents. Phantom validation results and maps of oxy-hemoglobin, deoxy-hemoglobin, water content, reduced scattering, and surface topography will be presented for pilot studies assessing burn severity and efficacy of port wine stain treatment.

Keywords: Spatial Frequency Domain Imaging, Multi-spectral imaging, DMD, Modulated Imaging, tissue optics

INTRODUCTION

Quantitative characterization of tissue structure and function is one of the most challenging problems in medical imaging. Optical methods can potentially provide a single platform for imaging biological tissues with resolution and depth sensitivity from microns to centimeters, limited by fundamental light-tissue interactions. Spatial Frequency Domain Imaging (SFDI) is a non-contact, wide-field imaging method [1, 2] which uses structured illumination coupled with a light propagation model to measure intrinsic tissue optical properties. The resulting data products are two dimensional maps of absorption (μ_a) and reduced scattering (μ_s') at discrete wavelengths. Combined with multi-spectral imaging at optimal wavelengths, this method is able to characterize tissue biochemical composition by quantitatively mapping oxy-hemoglobin (ctO_2Hb), deoxy-hemoglobin (ctHHb), total hemoglobin (ctTHb), and tissue oxygen saturation (stO_2)[3]. SFDI can also quantify the reduced scattering coefficient which can give insight into structural changes in tissue. SFDI has been previously used to measure chromophores in volar forearm [1, 3], optical properties of tattooed skin [4], as well as pre-clinical and clinical tissue transfer flaps [5-7]. Herein, we present implementation of a new LED based clinical SFDI system.

MATERIALS AND METHOD

SFDI Method

The theory behind tissue optical property characterization and imaging in the spatial frequency domain has been described[1]. Briefly, SFDI uses spatially-modulated structured illumination patterns projected (Fig. 1a) onto tissue at various frequencies in the form:

$$S = \frac{S_o}{2}[1 + M_0 \cos(2\pi f_x + \alpha)] \quad (1)$$

where S_0, M_0, f_x, and α are the illumination source intensity, modulation depth, spatial frequency, and spatial phase, respectively. The remitted light, I, from the sample is captured by a CCD camera and is composed of AC and DC components

$$I = I_{AC} + I_{DC} \quad (2)$$

The measured AC component of the remitted intensity, I_{AC}, can be characterized as:

$$I_{AC} = M_{AC}(x, f_x) * \cos(2\pi f_x + \alpha) \quad (3)$$

where $M_{AC}(x,fx)$ represents the modulation of diffusively reflected photon density waves (PDW) which in turbid media depend on the optical properties of the tissue and can be modeled with diffusion based or Monte Carlo based light transport methods[1]. In order to extract $M_{AC}(x,fx)$, a signal demodulation method is used. The sample is illuminated with a sinusoidal pattern at a specific spatial frequency with three phase offsets α=0, 2π/3, and 4π/3 radians (Fig. 1a). $M_{AC}(x,fx)$ is then calculated using the demodulation expression:

Emerging Digital Micromirror Device Based Systems and Applications IV, edited by Michael R. Douglass, Patrick I. Oden,
Proc. of SPIE Vol. 8254, 82540A · © 2012 SPIE · CCC code: 0277-786X/12/$18 · doi: 10.1117/12.909813

$$M_{AC}(x, f_x) = \frac{\sqrt{2}}{3}[(I_1 - I_2)^2 + (I_2 - I_3)^2 + (I_3 - I_2)^2]^{1/2} \qquad (4)$$

In order to calculate tissue optical properties, $M_{AC}(x,fx)$ can be measured using three phase projection images at a high spatial frequency (f_x > 0.1 mm^{-1}) and planar illumination or low spatial frequency (f_x = 0 mm^{-1}). The patterns are projected at multiple phases over the sample and demodulated using equation 4. The diffuse reflectance is then calculated at each spatial frequency using a silicone calibration phantom of known optical properties. This calibration corrects for any system response due to spatial variation of the illumination light and lens blurring. The sample height is calculated using sinusoid phase information and the reflectance is calibrated using an algorithm described previously[8]. Finally, these data is fit at each pixel to a known look-up table (LUT) created with a forward Monte Carlo model[1]. An LUT allows for relatively rapid visualization of optical property maps (~10 s).

In order to measure intrinsic biological chromophores such as oxy- and deoxy-hemoglobin, the scattering corrected optical absorption maps are measured at discrete wavelengths using SFDI. In general, the optical absorption at a single wavelength, μ_a, can be characterized by:

$$\mu_a(\lambda_i) = \sum_{n=1}^{N} \varepsilon_n(\lambda_i) c_n \quad (5)$$

where μ_a, $\varepsilon_n(\lambda_i)$, c_n, and N represent the optical absorption coefficient, chromophore extinction coefficient at a given wavelength, chromophore concentration, and number of chromophores, respectively. With a priori knowledge of the extinction coefficient matrix, $\varepsilon_n(\lambda_i)$ and measurements of the absorption coefficient at multiple wavelengths, the concentration, c_n, of each chromophore can be extracted using Equation 5. Typical basis spectra for tissue chromophores have been measured and characterized by multiple researchers and are used here[9]. A summary of the method is shown in Figure 1.

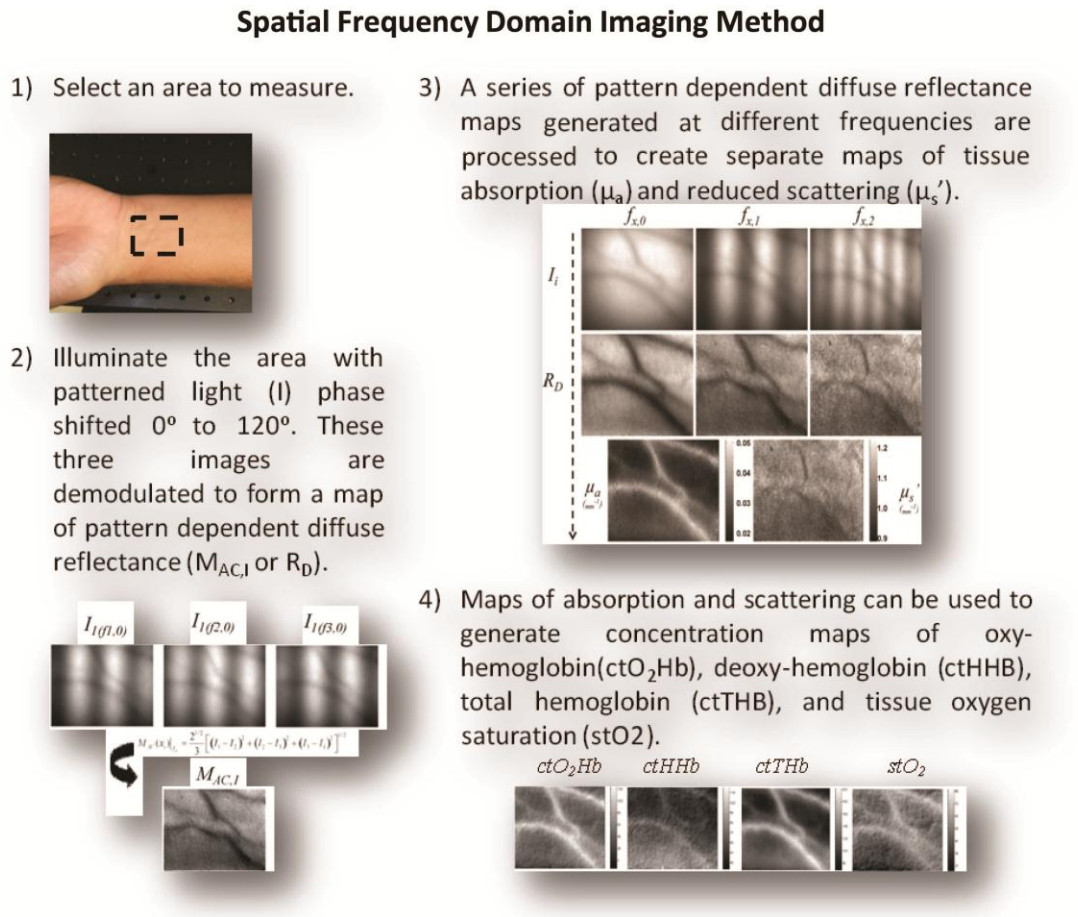

Figure 1. SFDI Method

Instrumentation

A typical SFDI instrument consists of three fundamental components: a light source, spatial light modulator and camera. A typical laboratory SFDI set-up is shown in Figure 2(a) and the overall size can be estimated to be about 10 cubic feet. Although, this instrument has been used in some clinical proof of concept studies, there was a need for a compact high throughput version. For these studies, a prototype clinic-compatible system (Modulated Imaging Inc., Irvine, CA) was used to measure ctO_2Hb, ctHHb, and stO_2. The imaging head is contained in a compact enclosure (~ 7' x 8' x 11') and light-weight (~ 12 lbs) enough to be mounted on an articulating arm attached to a portable cart as shown in Figure 2(b). As explained above, the SFDI system must have multi-spectral imaging capabilities to extract tissue chromophore concentrations. Based on previous work[3], a light source consisting of modules with LED's centered at 658, 730, 850 and 970 nm have been implemented in this system to optimize quantification of the chromophores listed above [3]. The projection optics are optimized for the near infrared and typical exposure times are 10 ms for the shorter three wavelengths (658 nm, 730 nm, 850 nm) and 200ms for 970 nm. These exposure times reduce typical acquisition time to seconds making the system approximately twenty times faster than the SFDI system that we have described previously (Fig. 2a) while minimizing the effect of motion artifacts in the clinic. A digital light projector based on a Digital Micromirror Device (Texas Instruments DMD Discovery™ 1100) is used to project patterns for large field of view applications (13.5 cm x 10.5 cm). The detection arm consists of two cameras: a dedicated near-infrared (NIR) camera and a color camera. White light is projected after each pass of data to capture a color photograph of the region of interest so that SFDI data can be compared at the exact same site on human skin before and after laser treatment. The projector and NIR detection arms are fitted with cross-polarizers to eliminate specularly reflected photons. All system hardware is controlled by custom C# software (Modulated Imaging Inc., Irvine, CA) connected to a PC computer via universal serial bus (USB). In addition to SFDI data, a surface profilometry measurement is built into the acquisition in order to correct for optical property errors resulting from surface curvature, as described by Gioux *et al* [8]. Optical property determination, chromophore concentration map rendering, and image processing are done using MATLAB (the MathWorks, Natick, MA), which occurs off-line, after data has been acquired. Prior hardware configurations were primarily focused on method development and flexibility to allow for a variety of imaging, projection and light source subsystems.

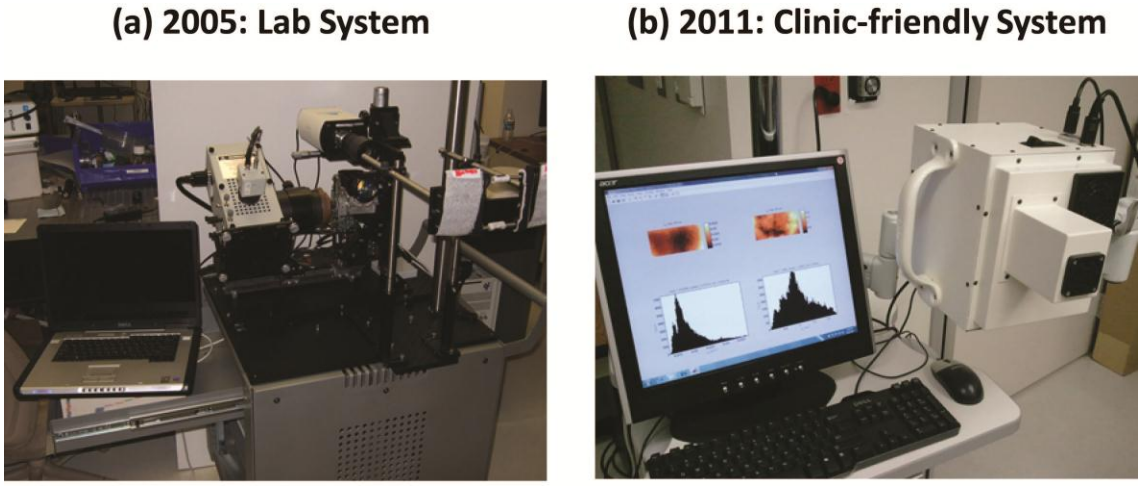

Figure 2. Evolution of SFDI systems

RESULTS

Time Course Phantom Validation of System

A series of testing protocols were created to evaluate system performance in a laboratory setting. Protocols for assessing short- and long-term optical and spectral stability, projection homogeneity, signal-to-noise, optical property precision, effects of curved surfaces on recovered indices have been formalized and documented. In order to evaluate the optical stability of clinic-friendly LED system, time course data was taken of a homogenous phantom (μ_a ~ 0.017 mm^{-1}, μ_s' ~ 1 mm^{-1} @ 658 nm) with a typical measurement sequence setting. Data was calibrated to first time point and then optical properties were calculated subsequently with data passes every 30 seconds. As shown in Figure 3, the spatial variation in the images is minimal. The color bar for the absorption map at 658nm after 20 minutes ranges from +/- 3% and is extremely close to expected value. The recovered mean absorption and scattering values at 658 nm in four regions of interest (ROIs) match expected values. The standard deviations (error bars on plots) for these ROIs show a 2% variation in recovered optical properties. However, the mean drift of optical properties is less than 1% for both absorption and scattering over the time course measurement.

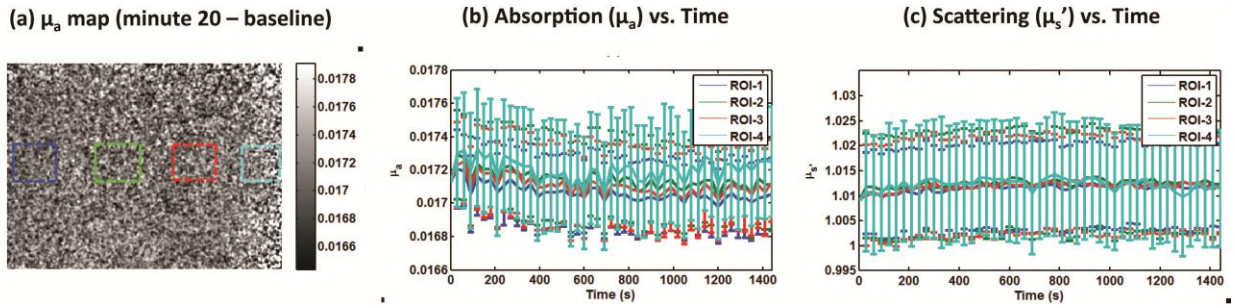

Figure 3. Spatial drift characteristics of clinic-friendly LED system over 30 minutes

Similarly, this phantom was analyzed for all remaining LED wavelengths. In Figure 4, we see the system is stable and less than 1% intensity drift is measured over time for all wavelengths. There is a slight deviation at 970nm at approximated 750s. This is most likely due to fluctuation in room light. 970nm is by far the weakest source and requires the longest integration time. Thus, it can be sensitive to any changes in ambient lighting compared to the lower three wavelengths.

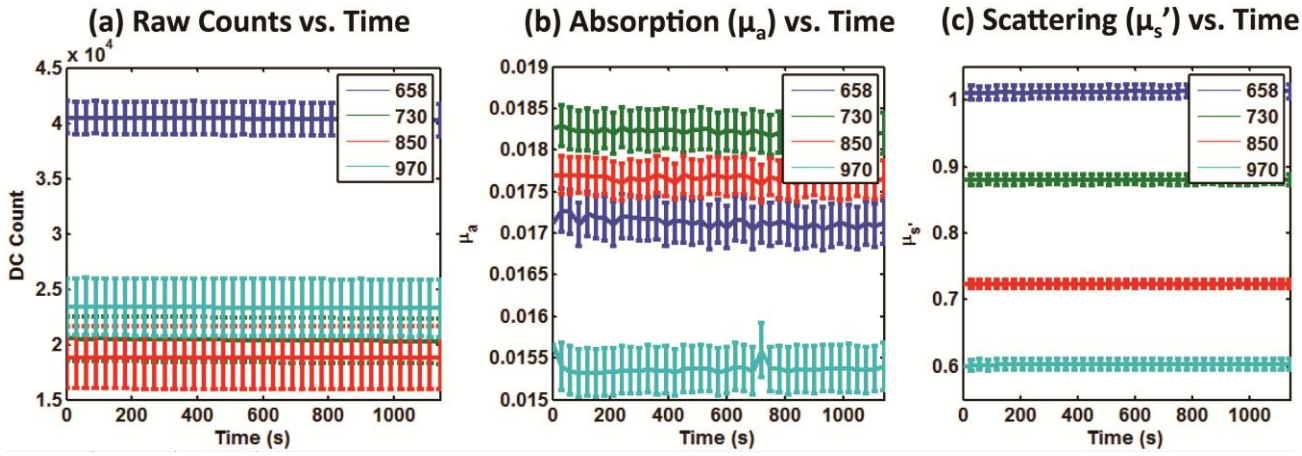

Figure 4. Drift characteristics of an ROI in image clinic-friendly LED system for all wavelengths over 30 mins.

Blood Phantom Measurements

Another example of a test module was to confirm the clinic-friendly device's ability to measure blood volume and tissue saturation. In this module, tissue-simulating phantoms were fabricated with fluid emulsions of a 20 fold dilution of 20% intralipid (Baxter Healthcare, Deerfield, IL) mixed with isotonic phosphate buffered saline (PBS) solution adjusted to a pH of 7.4 at 37°C. Phantom absorption was achieved by adding intact porcine erythrocytes. The dissolved oxygen content was measured using a dip-type oxygen microelectrode (MI-730, MicroElectrodes Inc., Bedford, NH) which was used as a gold standard. The phantom was then slowly deoxygenated by adding 0.3g of dry baker's yeast after blood was well mixed and oxygenated in phantom. SFDI-derived time course maps of ctO_2Hb, ctHHb, and stO_2 are shown in Figure 5. A clear exchange in ctO_2Hb and ctHHb values is evident after yeast was added to phantom. The partial pressure of oxygen measured by the electrode was plotted against extracted tissue saturation from LED SFDI device to generate a hemoglobin-oxygen disassociation curve (not shown). The recovered Hill curve parameters showed strong agreement with previous literature[10].

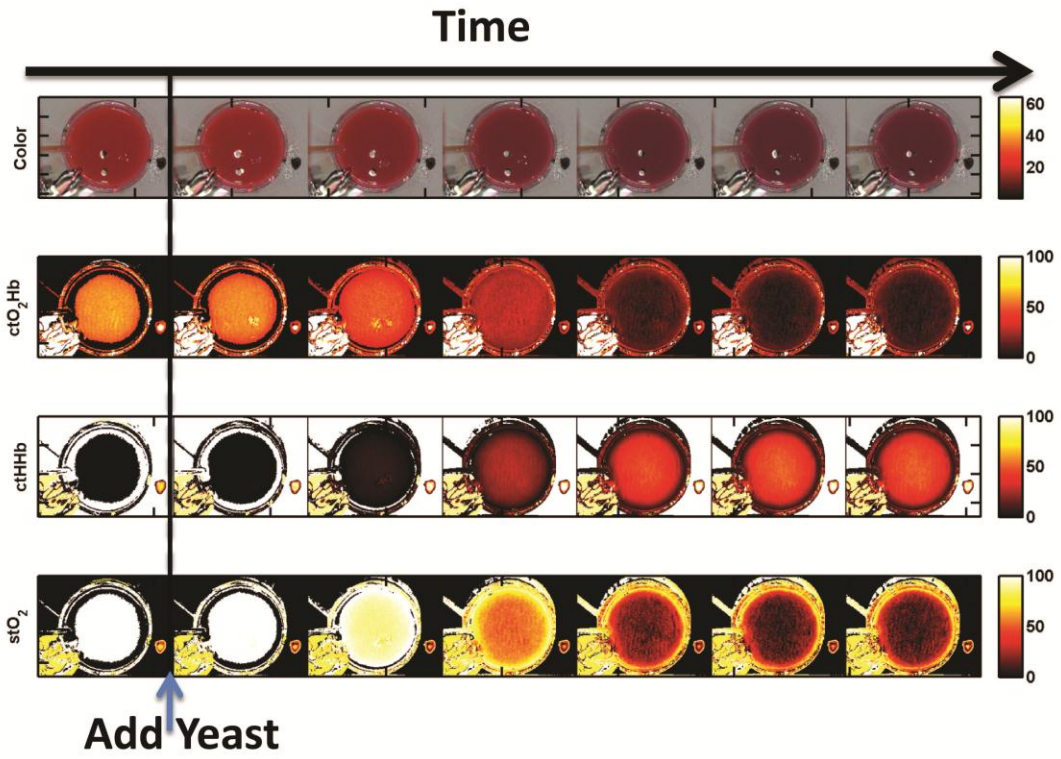

Figure 5. Recovered SFDI maps of blood phantom deoxygenation

Preliminary In vivo Measurements – Port Wine Stains

Port wine stain (PWS) birthmarks are congenital progressive vascular malformations that typically occur on the head or neck [11]. These lesions are difficult to conceal and are often the cause of physical and emotional disability due to facial asymmetry and deformity [12]. Pulsed dye laser (PDL) therapy with epidermal cooling is the current standard approach to treat these birthmarks by enabling destruction of abnormal subsurface blood vessels without significant damage to the epidermis. Objective methods to assess port wine stain (PWS) response to laser treatment have been the subject of various research efforts for several years[13]. Herein, we present preliminary data using our clinic-friendly SFDI device to record quantitatively biochemical compositional changes in PWS after laser therapy. The female patient (age 12) was recruited from an outpatient population at the Beckman Laser Institute and Medical Clinic, University of California, Irvine (UCI) in compliance with IRB approved protocol (#2010-7276). The PWS lesion was located on the face and the subject was asked to lie down supine on a gurney prior to measurement in order to minimize movement artifacts. The PWS lesion was measured prior to, and immediately, after laser treatment. SFDI derived optical property data and chromophore concentration data for subject 1 measured on the PWS as compared to normal skin are shown in figure 6. As shown in the data, elevated levels of ctTHb and stO_2 are seen in lesion pre-treatment compared to normal skin. However, an increase in ctHHb, ctTHb, and decrease in stO_2 is evident immediately after treatment. The dramatic increase in ctHHb within PWS lesions after laser treatment occurs when the vasculature is compromised and red blood vessels leaks into the surrounding perivascular tissue. Purpura is a subjective visual sign used by surgeons to determine the endpoint of a single PWS lesion treatment. However, the utility of purpura as a clinical endpoint remains incompletely understood. We expect that with further investigation, SFDI may become a quantitative tool to assess clinical endpoint of a single treatment.

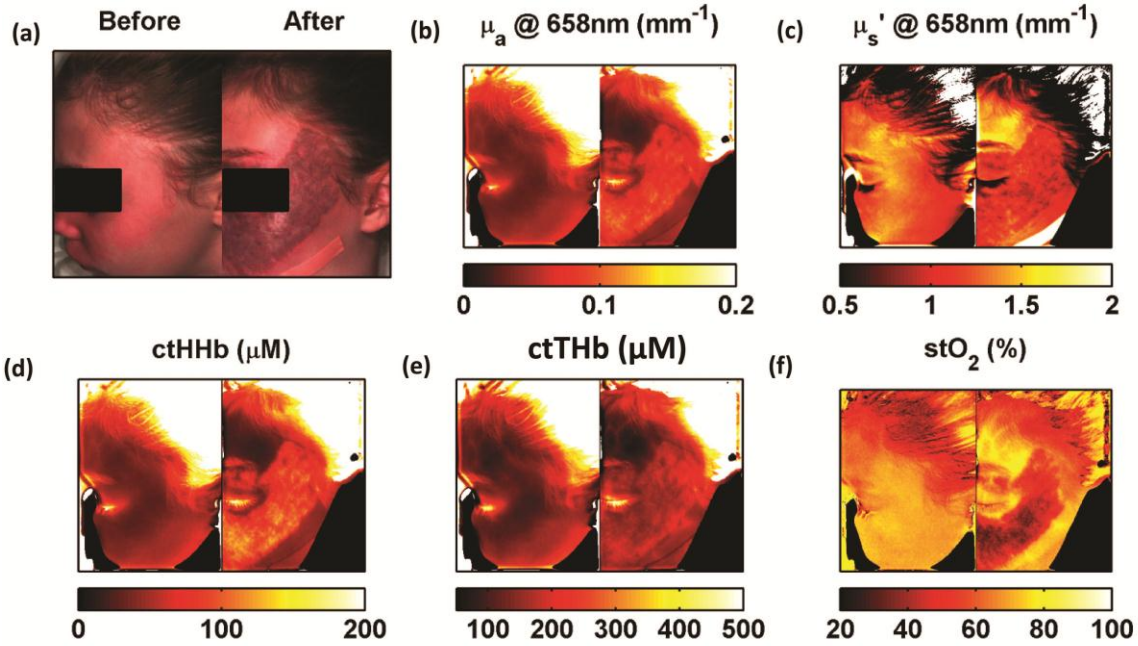

Figure 6. SFDI derived PWS data for subject 1 (measurement 1a). Collage of pre-operative (left) and postoperative (right) (a) color images, (b) absorption map, (c) scattering map, (d) deoxy-hemoglobin map, (e) total hemoglobin map and (f) tissue oxygen saturation map. Elevated ctTHb and stO_2 are seen in lesion pre-treatment. An increase in ctHHb, ctTHb, and decrease in stO_2 is evident immediately after treatment.

Preliminary *In vivo* Measurement – Burns

Accurate determination of burn depth and extent, which is directly related to healing times, is one of the major problems that face any clinician or surgeon in deciding on how to treat skin burns[14]. Superficial burns are mild burns whereby the tissue is capable of regenerating the epidermis. Partial thickness injuries destroy a portion of the dermal layer and re-epithelialization can occur if there is sufficient dermis with an adequate vasculature. Full thickness injuries involve destruction of the dermal layer and the reduced blood supply will result in ischemia and necrosis. Superficial burns are typically treated with dressings and covered, whereas full thickness burns are excised and closed or grafted. Both the superficial and full-thickness burns are readily diagnosed and the most difficult to assess are the partial thickness burns. In this preliminary work, we are beginning to characterize the baseline optical properties of burn patients. In this example, we show an example of a patient with a deep burn in after five days of admittance. All imaging was done with informed consent and under IRB-approved protocol (#2009-7322) at the UCI Burn center. We see that in Figure 7, that there is minimal contrast in absorption at 850nm but the area with burned skin has reduced scattering in regions with burned skin. This could be due to structural changes in skin due to the burn event. Currently, we are still in the process of evaluating the differences in optical properties and chromophore concentration across a larger cross-section of patients with different skin types and burn depth and extents. We expect that with further evaluation, we may able to use SFDI to quantitatively evaluate both burn depth and extent and inform surgeon treatment.

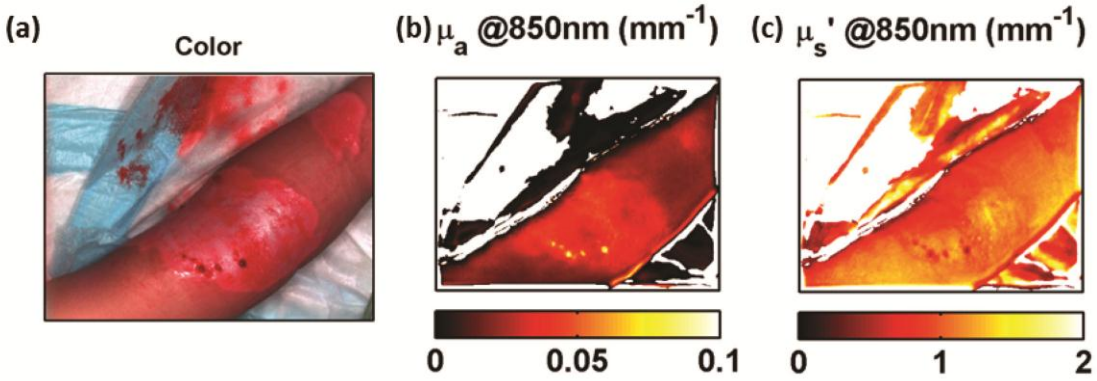

Figure 7. Preliminary SFDI recovered optical maps in a burn patient with a deep burn.

CONCLUSION

We have presented the first implementation of a new LED based clinical SFDI system for large field of view imaging. This system is much smaller with improved light throughput and shorter acquisition times than its predecessor laboratory system. We have shown some phantom testing to validate the system over time. We have also presented preliminary validation of tissue oxygen saturation measurements in phantoms using this system. Finally, we presented two snapshots of preliminary clinical deployment in port wine stains and burn imaging.

ACKNOWLEDGEMENTS

The authors gratefully acknowledge funding provided by the NIH SBIRs 1R43RR030696-01A1**,** and 1R43RR025985-01**,** the NIH NCRR Biomedical Technology Research Center (LAMMP: 5P-41RR01192), the Military Photomedicine Program, AFOSR Grant # FA9550-08-1-0384, and the Beckman Foundation. The authors would like to thank Dr. John S. Nelson, Dr. Kristen Kelly, and Dr. Nicole Bernal for their assistance in preliminary clinical measurements.

REFERENCES

[1] S. Gioux, A. Mazhar, D. J. Cuccia *et al.*, "Three-dimensional surface profile intensity correction for spatially-modulated imaging," J Biomed Opt, 14(3), 034045 (2009).

[2] D. J. Cuccia, F. Bevilacqua, A. J. Durkin *et al.*, "Modulated imaging: quantitative analysis and tomography of turbid media in the spatial-frequency domain," Opt Lett, 30(11), 1354-6 (2005).

[3] A. Mazhar, S. Dell, D. J. Cuccia *et al.*, "Wavelength optimization for rapid chromophore mapping using spatial frequency domain imaging," Journal of Biomedical Optics, 15(6), 061716-061716 (2010).

[4] F. R. Ayers, D. J. Cuccia, K. M. Kelly *et al.*, "Wide-field spatial mapping of in vivo tattoo skin optical properties using modulated imaging," Lasers Surg Med, 41(6), 442-53 (2009).

[5] S. Gioux, A. Mazhar, B. T. Lee *et al.*, "First-in-human pilot study of a spatial frequency domain oxygenation imaging system," J Biomed Opt, 16(8), 086015 (2011).

[6] M. R. Pharaon, T. Scholz, S. Bogdanoff *et al.*, "Early detection of complete vascular occlusion in a pedicle flap model using quantitation spectral imaging," Plastic and reconstructive surgery, 126(6), 1924-35 (2010).

[7] A. Yafi, T. S. Vetter, T. Scholz *et al.*, "Postoperative quantitative assessment of reconstructive tissue status in a cutaneous flap model using spatial frequency domain imaging," Plastic and reconstructive surgery, 127(1), 117-30 (2011).

[8] S. Gioux, A. Mazhar, D. J. Cuccia *et al.*, "Three-dimensional surface profile intensity correction for spatially modulated imaging," Journal of Biomedical Optics, 14(3), 034045-034045 (2009).

[9] W. G. Zijlstra, A. Buursma, and W. P. Meeuwsen-van der Roest, "Absorption spectra of human fetal and adult oxyhemoglobin, de-oxyhemoglobin, carboxyhemoglobin, and methemoglobin," Clin Chem, 37(9), 1633-8 (1991).

[10] J. C. Finlay, and T. H. Foster, "Recovery of hemoglobin oxygen saturation and intrinsic fluorescence with a forward-adjoint model," Appl Opt, 44(10), 1917-33 (2005).

[11] B. Tallman, O. T. Tan, J. G. Morelli *et al.*, "Location of port-wine stains and the likelihood of ophthalmic and/or central nervous system complications," Pediatrics, 87(3), 323-7 (1991).

[12] A. Troilius, B. Wrangsjo, and B. Ljunggren, "Patients with port-wine stains and their psychosocial reactions after photothermolytic treatment," Dermatol Surg, 26(3), 190-6 (2000).

[13] K. M. Kelly, B. Choi, S. McFarlane *et al.*, "Description and analysis of treatments for port-wine stain birthmarks," Arch Facial Plast Surg, 7(5), 287-94 (2005).

[14] M. Kaiser, A. Yafi, M. Cinat *et al.*, "Noninvasive assessment of burn wound severity using optical technology: a review of current and future modalities," Burns, 37(3), 377-86 (2011).